https://ntrs.nasa.gov/search.jsp?R=19820005277 2020-03-21T10:00:19+00:00Z

N O T I C E

THIS DOCUMENT HAS BEEN REPRODUCED FROM MICROFICHE. ALTHOUGH IT IS RECOGNIZED THAT CERTAIN PORTIONS ARE ILLEGIBLE, IT IS BEING RELEASED IN THE INTEREST OF MAKING AVAILABLE AS MUCH INFORMATION AS POSSIBLE

PURDUE UNIVERSITY
SCHOOL OF AERONAUTICS AND ASTRONAUTICS

(NASA-CR-165036) INTERACTIVE AIRCRAFT FLIGHT CONTROL AND AEROELASTIC STABILIZATION Interim Report (Purdue Univ.) 39 p HC A03/MF A01 CSCL 01C
N82-13150
Unclas G3/08 08564

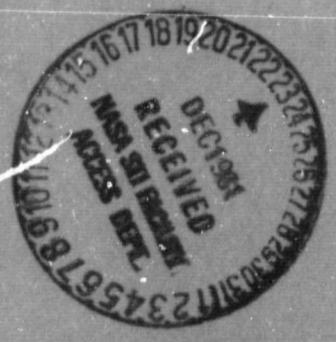

West Lafayette, Indiana 47907

Interactive Aircraft Flight Control and Aeroelastic Stabilization

NASA/Langley Research Center Grant-NAG-1-157

Interim Report-Body Freedom Flutter of Forward Swept Wings

Submitted by:

Dr. Terrence A. Weisshaar
Principal Investigator

and

Dr. David K. Schmidt
Associate Professor

School of Aeronautics and Astronautics
Purdue University
West Lafayette, Indiana

SUMMARY

This report presents several examples in which flutter involving interaction between flight mechanics modes and elastic wing bending occurs for a forward swept wing flight vehicle. These results show the basic mechanism by which the instability occurs and form the basis for attempts to actively control such a vehicle. This work was accomplished between 1 May 1981 and 31 October 1981.

INTRODUCTION

It has been known for many years that the calculated flutter speed of an aircraft may be modified by the inclusion of the rigid body or free-free modes of the aircraft. Similarly, the predicted aircraft stability and control characteristics may be significantly different if structural flexibility is included in the analysis. Over the years, certain informal guidelines have been developed to assess the potential importance of the body-freedom modes to flutter analysis.

The earliest report on the subject of body-freedom influence on flutter appears to be due to Frazer and Duncan (Ref. 1). Their study showed that "fuselage mobility" had a slightly favorable effect on the calculated flutter speeds. Broadbent (Ref. 2) discussed the necessity for the inclusion of the body-freedoms for swept wing flutter calculations. Gaukroger (Ref. 3, 4) also conducted several significant investigations into the influence of body-freedom on flutter. His studies are summarized in the AGARD Manual on Aeroelasticity (Ref. 5). His studies revealed that, when body-freedoms are included in the analysis, two distinct types of symmetric flutter can occur. The first type of flutter results from wing bending coupling with body pitch. Gaukroger uses the term "body-freedom flutter" to describe this phenomenon. He further notes that the flutter speed for this type of flutter may be low when compared to the flutter speed computed without body freedoms included. In addition, the reduced frequency at which body freedom flutter occurs is also relatively low. Measured in terms of wing chord lengths traveled by the aircraft

during one oscillation cycle, this travel distance at the flutter speed is of the order of 100 chord lengths per cycle. These oscillations are well within the range of interest of flight mechanics specialists.

The second type of symmetric flutter that can occur with body-freedom included is relatively insensitive to fuselage inertia. This type of flutter resembles that obtained when the wing root is held fixed. The critical speeds, mode shapes, and frequencies are very nearly the same for the body-freedom and fixed root analysis. Gaukroger also determined that the presence of the horizontal stabilizer had a favorable effect on the body-freedom flutter speed. Gaukroger's results were confined to the aft sweep region.

An additional, definitive, report on the subject of body-freedom flutter is given in Ref. 6 by Cunningham and Lundstrom. In Ref. 6, an analysis is presented to predict the flutter speed of a sounding rocket with an unswept wing. Since their results have a direct bearing upon the results presented later in this report, we will review them here.

The Cunningham/Lundstrom structural dynamic model of the sounding rocket included four degrees of freedom.

(1) Wing bending in the fundamental mode.

(2) Wing torsion in the first mode.

(3) Fuselage pitch

(4) Fuselage plunge

Unsteady aerodynamic effects are introduced via the familiar Theodorsen aerodynamic theory used in conjunction with aerodynamic strip theory.

Their analysis found two critical flutter roots. The first was a body-freedom root, while the second was a wing bending-torsion root. The former occurred at a frequency of 26% of the bending frequency, while

the latter occurred at 3.40 times the fundamental bending frequency. A significant result of their analysis was that wing position relative to the missile c.g. had an important effect on the value of the flutter velocity. As the wing leading edge approached the c.g. the body-freedom flutter speed was increased. As the wing moved aft, the body-freedom flutter speed first declined, then slowly increased.

In Ref. 6, the importance of including various degrees of freedom was discussed. From the calculations performed by modeling the system as a binary or ternary system, it was concluded that the inclusion of rigid body plunge was important, in that it raised the flutter speed when compared to a similar computation excluding this degree of freedom. In addition, although wing bending stiffness rather than wing torsional stiffness was found to have the predominant effect on body-freedom flutter, including torsional flexibility lowered the flutter speed by about 14%.

Since static aeroelastic divergence can be characterized as flutter at zero frequency, we should be alert to the potential effects of body freedoms upon divergence. This problem is lucidly discussed by Hancock (Ref. 7) for the case of torsional divergence; the effect of static aeroelastic flexibility upon the aircraft stability and control problem is discussed in Ref. 8, also by Hancock. However, until recently the forward sweep bending divergence problem has not been considered.

The purpose of the present study is to attempt to identify the importance and the effects of the inclusion of body freedoms into a dynamic aeroelastic analysis of a symmetrical forward swept wing. For this study, we will employ a ternary model with body freedoms in pitch and plunge and a single fundamental bending mode. Torsion is deleted to isolate the effect of bending flexibility on the forward swept wing divergence problem. Our focus will be confined to the low frequency body freedom

flutter phenomena. The particular interest is the determination of where in the flight envelope body freedom flutter occurs relative to clamped wing divergence. For this reason, quasi-steady strip theory aerodynamics are employed since their mathematical representation is simple and relatively easy to interpret.

Model Parameters and Restrictions

The planform geometry of the aeroelastic stability analysis model is illustrated in Figure 1. The flexible wing has a uniform chord, c, and sweepback, Λ. The junction between the wing and fuselage is located a distance (denoted as the dimension x) aft of the aircraft c.g. The swept semi-span dimension of each wing is ℓ.

The model has three degrees of freedom; these are:

1) vertical displacement of the aircraft c.g., denoted as w, measured positive upward.
2) pitching of the fuselage about the c.g., denoted as θ, positive nose-up.
3) bending of the wings, measured with respect to the wing root, positive upward.

Motion is restricted to be symmetrical with respect to the fuselage centerline. This approach is essentially the same as that used by Pai and Sears (Ref. 9) to study the effect of wing bending upon aircraft longitudinal oscillation and by Cunningham and Lundstrom in the previously cited work. In the present analysis, however, the effects of an active canard/tail are included, since the presence of active controls can modify our conclusions.

Strip theory aerodynamics are used to describe the airloads present on the wings as they oscillate. These loads are assumed to be quasi-steady so that the aerodynamic influence coefficients are independent of reduced frequency.

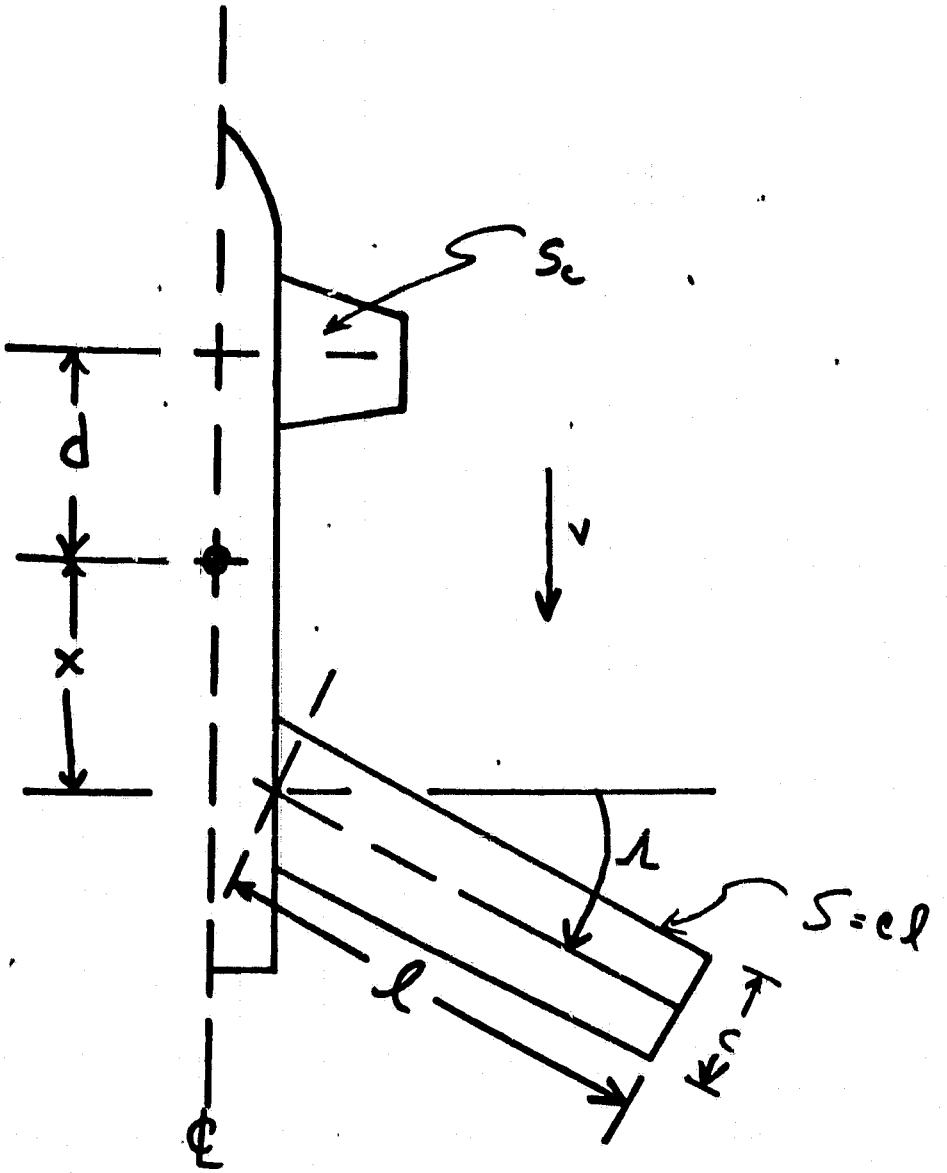

Figure 1 - Planform Geometry

Three equations are necessary to describe the motion of the aircraft model. These equations are developed in the Appendix. One equation describes the vertical motion of the aircraft center of gravity. A second equation describes the oscillatory behavior of the flexible wing, while the third equation is written to describe the pitch motion of the aircraft. These three equations contain differential operators and integrals (see the Appendix for details). By using Galerkin's Method, and suitable nondimensionalization, the equations can be written in matrix form. Several parameters arise from this nondimensionalization and will be discussed before proceeding further.

Body-freedom Flutter Parameters

With the assumptions and restrictions discussed previously, a set of parameters, some of them nondimensional, appear in the equations of motion. These parameters are as follows:

$\mu = 2\, m\ell / M_F$ = the wing/fuselage mass ratio. Note that the total mass of the aircraft is $M_F(1 + \mu)$.

$\bar{y} = \frac{x}{\ell} + \frac{\sin\Lambda}{2}$ = the longitudinal distance from the aircraft c.g. to a wing center span, measured in swept wing lengths. See Figure 1.

$M_T = M_F + 2\, m\ell$ = total mass of the aircraft.

$= (1 + \mu)\, M_F$

$I_p = M_T\, r^2$ = the aircraft mass moment of inertia in pitch, measured about the aircraft c.g.

$\bar{r}^2 = \left(\frac{r}{\ell}\right)^2$ = aircraft radius of gyration, squared, divided by ℓ^2.

$S = c\ell$ = wing area of one wing

$C_{L\alpha}$ = wing lift curve slope

ω_o = natural frequency in bending for the wing with the fuselage fixed, in radians per second.

$q_n = \frac{1}{2} \rho V^2 \cos^2 \Lambda$, dynamic pressure parameter.

$V_n = V \cos \Lambda$, the air speed component normal to the wing leading edge.

With the assumption that the time dependence of the motion is e^{st}, the equation for the dynamic response of the model is

$$[s^2[M] + s[B] + [K]] (\zeta) = (F) \qquad (1)$$

where

$$\zeta_1 = \bar{w}/\ell$$

$$\zeta_2 = \bar{h}/\ell$$

$$\zeta_3 = \bar{\theta}$$

and $\bar{w}$, $\bar{h}$ and $\bar{\theta}$ are modal amplitudes of the three distinct types of motion. The three matrices, [M], [B] and [K] are defined in the Appendix.

The mass matrix [M] is nondimensional and contains cross-coupling terms. These coupling terms are functions of the mass ratio μ, the sweep angle Λ and the longitudinal distance between the aircraft c.g. and the single wing semi-span. One would suspect that, as in all flutter problems, the mass coupling plays an important role in either controlling flutter or triggering flutter. In particular, the coupling term M_{23} describes the inertia coupling between wing bending and fuselage pitch. It will be shown later that this term can be positive, negative or zero, depending upon the wing longitudinal position $\bar{x}$ and the sweep angle Λ.

The aerodynamic damping matrix [B] is symmetrical. It is composed of nondimensional terms that are functions of $\bar{x}$ and sin Λ. It, too, is fully populated. The damping matrix has a common factor, called D in the analysis.

$$D = \rho V_n \, SC_{L\alpha}/M_T \qquad (2)$$

The stiffness matrix is composed of the structural stiffness of the wing with respect to the fuselage and aerodynamic stiffness terms. The structural stiffness consists of a single term in the diagonal position associated with the wing bending mode deflection $\bar{h}$. The aerodynamic stiffness matrix is a function of sweep, Λ, wing position $\bar{x}$ and a common factor, Q.

$$Q = 2q_n \, SC_{L\alpha}\ell/M_T\ell \tag{3}$$

The aerodynamic stiffness matrix has several interesting features. The first column, associated with aircraft plunge, consists entirely of zeros. This is consistent with the fact that a small change in altitude does not alter the lift. If only the K_{22} term is retained, corresponding with the assumption that the fuselage is fixed, then static aeroelastic divergence will occur when the wing is swept forward. This divergence occurs at

$$q_D = \frac{-6.356 \, EI'}{C_{L\alpha} \, S\ell^2 \sin \Lambda \cos \Lambda} \tag{4}$$

The above coefficient of -6.356 is in excellent agreement with the exact solution for which the coefficient is -6.33. The difference occurs because the assumed bending mode shape used in the analysis is a polynomial and not the exact solution.

In addition, the fact that the aircraft system stiffness matrix has cross coupling terms proportional to dynamic pressure reminds us that the classical wing divergence problem must be modified in the case of the freely flying aircraft. Aeroelastic divergence will occur when the aerodynamic loads cause the stiffness matrix to become singular. This subject will be discussed later, but two points will be made now. First, in our model, the plunge degree of freedom plays no role in the determination of

aircraft divergence because of the column of zeros associated with this degree of freedom. This degree of freedom is always neutrally stable with respect to small perturbations as long as v remains constant. Second, the presence of the canard/tail alters the problem, as does wing placement. This is so because these parameters introduce cross-coupling in the stiffness matrix and these terms appear in the characteristic equation used to determine divergence.

The Model for an Active Canard

A model of an all-movable canard was also developed. The geometry of this canard is shown in Figure 1. The effect of this canard is assumed to be aerodynamic only. Any dynamic or inertial effects are ignored. With quasi-steady aerodynamic theory the canard aerodynamic forces and moments appear explicitly only in the c.g. and pitch equations of motion. The quasi-steady angle of attack of the canard surface is:

$$\alpha_c = \Theta + \delta_o - \left(\frac{\dot{w}}{v} + \frac{d\dot{\Theta}}{v}\right) \tag{5}$$

It is recognized that the aerodynamic interaction between the canard and the wing is considerably more complex than that just described. However, this approach provides at least a starting point for the discussion of active control of the aircraft with a canard.

The presence of a canard/tail control surface will add terms to the right hand side of our equations of motion. These terms fall within two categories: terms dependent upon the aircraft degrees of freedom $\{\zeta_i\}$; and terms depend upon the canard deflection, δ_o. The terms that are dependent upon the aircraft freedoms must be transferred to the left hand side of the equation of motion. Thus, the canard will now influence our aeroelastic stability problem, even when it is not active. The term proportional

to δ_0 can be made to be a function of (ζ) by defining a feedback control law. This potential for improving the vehicle aeroelastic stability will be discussed later.

The important parameters for the canard are called $\bar{d}$ and f in the analysis. These terms are defined as:

$$\bar{d} = d/\ell \quad \text{(see Figure 1)}$$

$$f = \left(\frac{S_c}{S}\right)\left(\frac{C_{L\alpha c}}{C_{L\alpha}}\right)$$

where S_c is the effective canard area and $C_{L\alpha c}$ is the canard lift curve slope.

The Effect of Wing Position Relative to the Aircraft C.G.

To illustrate the potential effect of wing position upon body freedom flutter, we will define an aircraft configuration typical of a fighter aircraft. It should be noted at the outset that the parameters chosen are typical of suggested designs for FSW fighters. Any resemblance to a specific design is coincidental. The parameters chosen are as follows:

$C_{L\alpha}$ (1/rad.)	μ	$\bar{d}$	f	$\bar{r}_0$ (Fuselage)	ω_0 (rad/sec.)	ℓ (ft.)	$M_T/2S$ (slugs/ft^2)	Λ (deg.)
6.28	0.11	0.3	0.17	0.61	68.0	15	3.8	-30

We begin our study by placing the wing in a far aft position with respect to the c.g., $\bar{x} = 0.45$. We will display our eigenvalue analysis results in root-locus format for clarity. The "gain" in this case will be dynamic pressure, q. No attempt will be made to correct the aerodynamic representation for Mach number effects, even though speeds are considerable.

Let us first focus on the eigenvalue root that begins as the pitching or "short period" mode. This root begins at the origin since, without

dynamic pressure, the pitching mode is neutrally stable. A root-locus plot of this short period root is shown in Figure 2 for a number of dynamic pressure values. The root is oscillatory and well damped until a velocity equal to about 0.8 V_{DC}, where V_{DC} is the clamped wing divergence speed. Up until this velocity, this mode has been acquiring a significant amount of bending deflection. After 0.8 V_{DC}, the root begins to move rapidly towards the right half plane as velocity is increased. At V = 0.89 V_{DC}, the root becomes unstable at a frequency of 22.37 rad/sec. corresponding to a reduced frequency of $k = \omega b/V = 0.026$.

The examination of the flutter mode reveals that at the time that the bending displacement reaches its maximum upward value ($\bar{h} = 1.0$), the aircraft plunges downward 0.55 units while the aircraft pitches upward 9.8 degrees. Upward fuselage motion lags upward bending by 174 degrees while nose up pitch leads by about 8 degrees.

Accounting for different coordinate definitions, these results are similar to those observed by Cunningham and Lundstrom for their rocket.

Turning to the bending mode behavior, we see in Figure 3 that this mode is more highly damped than the pitch mode. At about 0.8 V_{DC} this mode begins to develop highly damped oscillatory characteristics. An increase in dynamic pressure is seen to drive the frequency of the bending mode down, while the pitch mode frequency is increased. A classical frequency coalescence occurs, resulting in one mode becoming unstable. As velocity is increased slightly beyond 1.0 V_{DC}, the bending mode contacts the real axis in Figure 3. After this point, the eigenvalues for this mode are no longer complex conjugates, but are real and distinct. One root moves left, in the direction of increasing stability, while the other rapidly moves right with increasing velocity. As this root enters the right half plane at the origin, aircraft divergence occurs.

Fig. 2

ROOT LOCUS PLOT OF
PITCH BRANCH
$\bar{X} = 0.45$, $\Lambda = -30°$
LABELLED POINTS
INDICATE V/V_{DC} RATIOS.

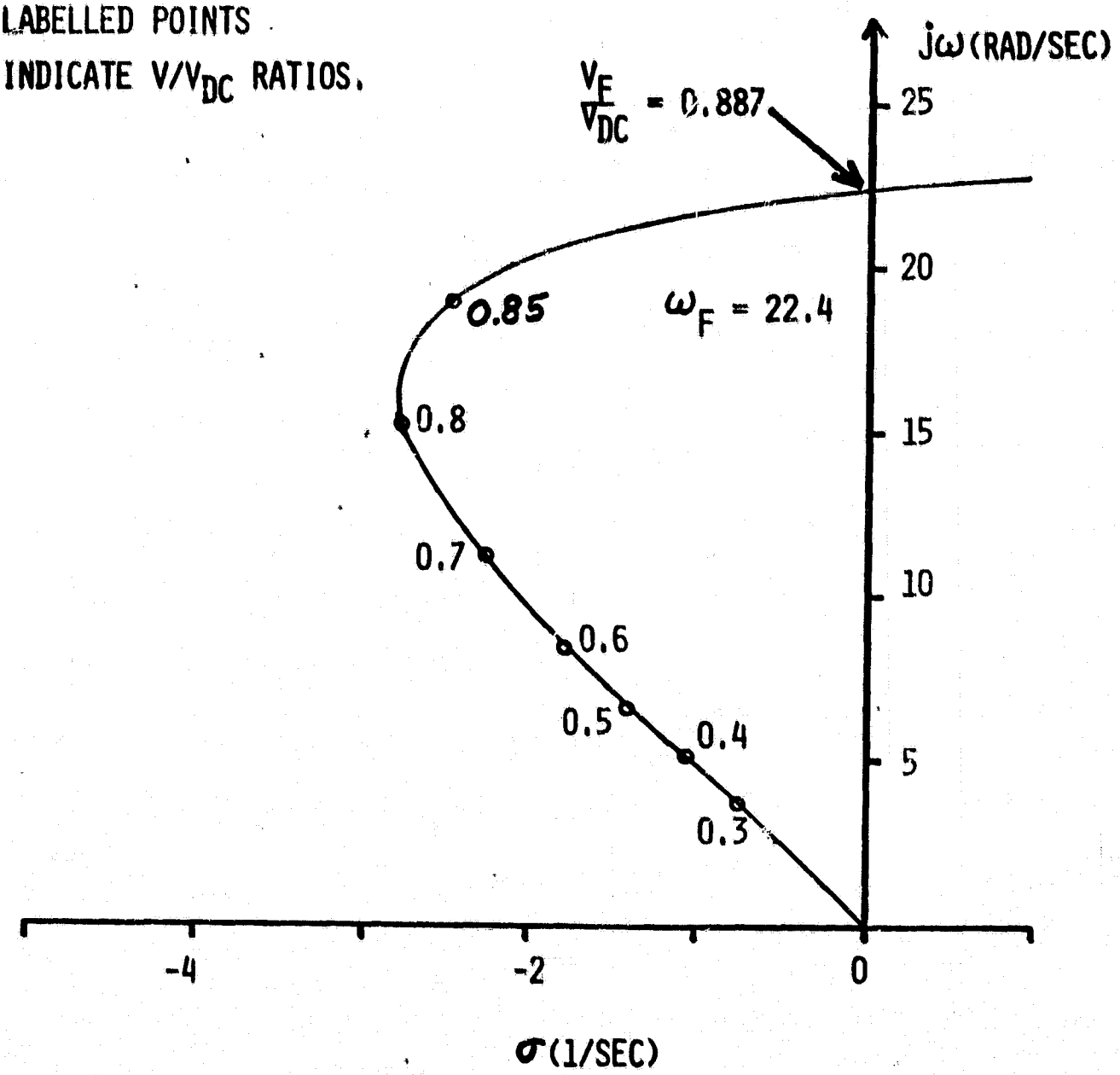

Figure 3

BENDING MODE ROOT LOCUS
WITH $\bar{X} = 0.45$
CIRCLES INDICATE VALUES
OF V/V_{DC}

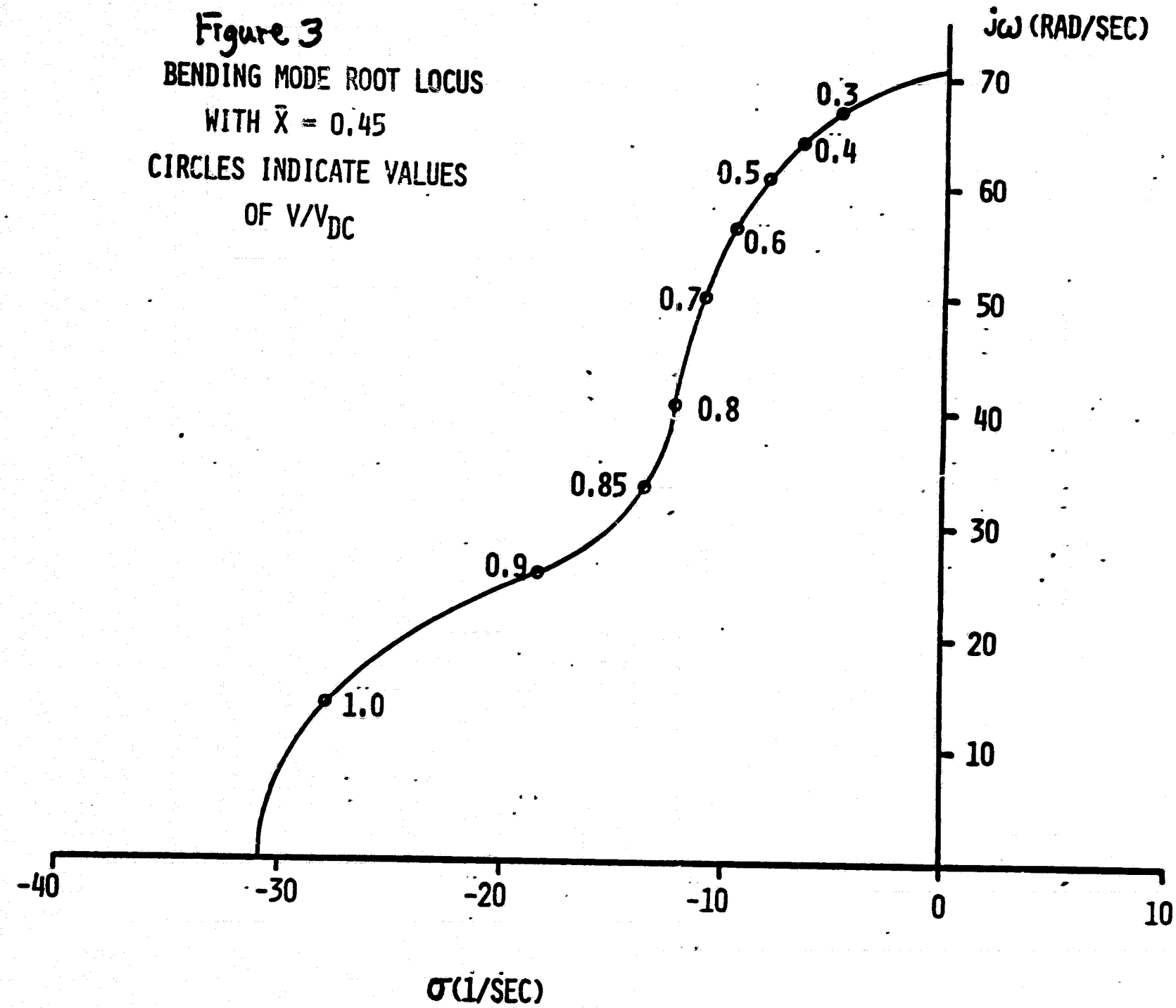

AIRCRAFT DIVERGENCE

Unlike clamped wing divergence, where the aircraft is restrained against motion, aircraft aeroelastic divergence involves wing bending and fuselage pitching. Mathematically, the eigenvalue problem that determines aircraft aeroelastic divergence comes from the requirement that, at divergence, the total stiffness matrix, including aerodynamic and structural effects, must be singular. The eigenvalues are related to the dynamic pressure. In terms of an eigenvalue solution for the dynamic equations, this divergence solution is valid if $s = 0$.

For a particular planform geometry, and with given aerodynamic characteristics and structural stiffness (in our case, this stiffness is characterized by the value of the root-fixed bending frequency), the three degree of freedom model will yield three values of q for which the system is neutrally stable. One of these values is zero, the second is undefined, while the third value is a function of the previously mentioned variables.

The zero flight dynamic pressure value indicates that the aircraft is neutrally stable in pitch if there is no forward speed. This occurs because an aerodynamic moment about the c.g. provides a "pitch spring" that, in turn, provides the restoring moment if the system is perturbed in pitch. In addition, the system is neutrally stable in plunge at any dynamic pressure since there are no "plunge springs", aerodynamic or otherwise.

The third root is meaningful. With the definition that q_{DC} is the root-fixed divergence speed, the aircraft aeroelastic divergence speed is q_{DA}, given by:

$$q_{DA} = q_{DC} \left[\frac{5(\bar{y} \cos \Lambda - \bar{d}f)}{(\bar{y} \cos \Lambda - 5\, \bar{d}f - 0.4 \sin \Lambda \cos \Lambda)}\right]$$

$$\frac{V_{DA}}{V_{DC}} = \left[\frac{5(\bar{y}\cos\Lambda - \bar{df})}{(\bar{y}\cos\Lambda - 5\,\bar{df} - 0.4\sin\Lambda\cos\Lambda)}\right]^{1/2}$$

where $\bar{y} = \bar{x} + \frac{\sin\Lambda}{2}$.

There appear to be two limiting cases for the above formula. If a tail is used, then $\bar{df}$ is less than zero. As $\bar{df}$ increases, due either to the use of a large horizontal stabilizer or a long tail length, the ratio V_{DA}/V_{DC} approaches unity. On the other hand, when $\bar{df}$ is greater than zero, ratio of V_{DA}/V_{DC} is infinite when

$$\bar{df} = \frac{\bar{y}\cos}{5} - \frac{2}{25}\sin\Lambda\cos\Lambda$$

As $\bar{df}$ increases from this value, the aircraft divergence dynamic pressure becomes negative. At some value of $\bar{df}$ the airplane will be statically unstable. In this case, V_{DA}/V_{DC} is zero. As $\bar{df}$ increases, the ratio becomes more positive and finally approaches unity as $\bar{df}$ gets larger.

These limiting trends are identical to those observed by Zeiler in a more general theoretical study of FSW aircraft divergence. It is clear that the analysis of static instability must reflect the presence of a canard/tail and include the aircraft geometry.

The mode shape at aircraft divergence is given as:

$$\frac{\bar{\theta}}{\bar{h}} = \left(\frac{\bar{y} + \frac{1}{10}\sin\Lambda}{\bar{y}\cos\Lambda - \bar{df}}\right)\sin\Lambda\cos\Lambda$$

If the aircraft is stable, then the numerator is greater than zero. The denominator will be positive if the airplane is statically stable with the canard in place. In this case, a FSW aircraft will have an aircraft divergence mode consisting of upward wing bending and nose-down pitch ($\bar{\theta}/\bar{h} < 0$).

For the aircraft whose dynamic stability properties were discussed previously, the ratio V_{DA}/V_{DC} is 2.59, well above the clamped wing bending divergence speed. Thus, we can assume that body freedom flutter is critical, unless a high frequency flutter mode is present at a lower speed.

The Effect of Moving the Wing Root Forward

Figure 4 is a root-locus plot of the results of an eigenvalue analysis of the aircraft equations of motion. Both the bending mode and the pitching mode roots are illustrated as a function of velocity. In this example, $\bar{x} = 0.35$ so that the wing root has been moved 0.10ℓ forward of that shown in the previous example.

The striking difference between this example and that shown previously is that the "ancestry" of the unstable mode has its roots in the wing bending mode. Wing bending coupling introduced into the pitch mode stabilizes that mode and actually causes it to be highly damped.

A similarity between the present case and the previous case is that, despite its ancestry, the flutter mode still occurs at about the same frequency and still involves coupling among the three degrees of freedom. Significantly, however, the flutter speed has increased by nearly 9%. This case undoubtedly more closely represents an actual aircraft configuration with the wing center of pressure in close longitudinal proximity to the aircraft c.g.

Figure 4

ROOT LOCUS PLOTS OF BENDING AND PITCHING BRANCHES, $\Lambda = -30°$, $\bar{X} = 0.35$. LABELLED POINTS INDICATE V/V_{DC} RATIOS.

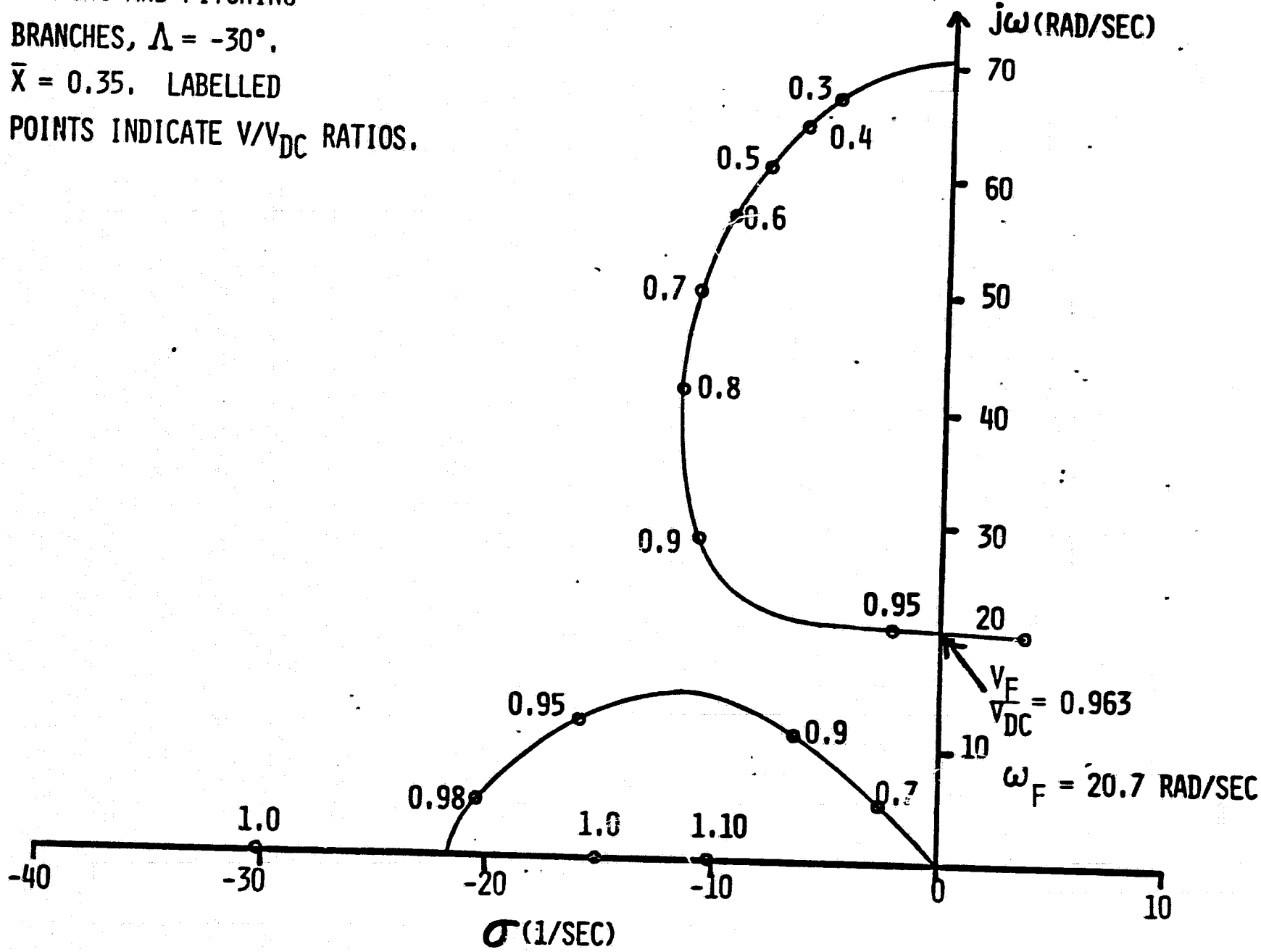

Some parameter has apparently changed significantly to cause the flutter mode to switch its ancestry. The bending mode has been modified so that it no longer contacts the real axis in the left half plane. There is still an aircraft divergence speed, but it is at 6.08 V_{DC}, and is associated with the pitching mode.

One significant difference between the $\bar{x} = 0.45$ case and the $\bar{x} = 0.35$ case is that the mass coupling term M_{23} has changed sign, from minus to plus, as the wing root moved forward. The expression for this term in the mass matrix is

$$M_{23} = \left(\frac{-\mu}{1+\mu}\right)\left(0.4\bar{y} + \frac{4}{45}\sin\Lambda\right) \tag{10}$$

This term is zero if $\bar{x} = \bar{x}_o$, where

$$\bar{x}_o = \frac{-13}{18}\sin\Lambda \tag{11}$$

For the 30 degree forward sweep case,

$$\bar{x}_o = \frac{13}{36} = 0.3611 \tag{12}$$

Figure 5 shows the root locus plot for the case where $\bar{x} = \bar{x}_o$. The critical mode still appears related to pitch mode instability. However, a distinct "pinching together" of the bending root and pitching root is apparent. Comparing Figure 5 to Figures 3 and 4,

Figure 5

ROOT LOCUS PLOTS OF BENDING BRANCH AND PITCHING BRANCH WHEN $M_{23} = 0$ ($\bar{X} = 0.3611$), $\Lambda = -30°$. LABELLED POINTS INDICATE V/V_{DC} RATIOS.

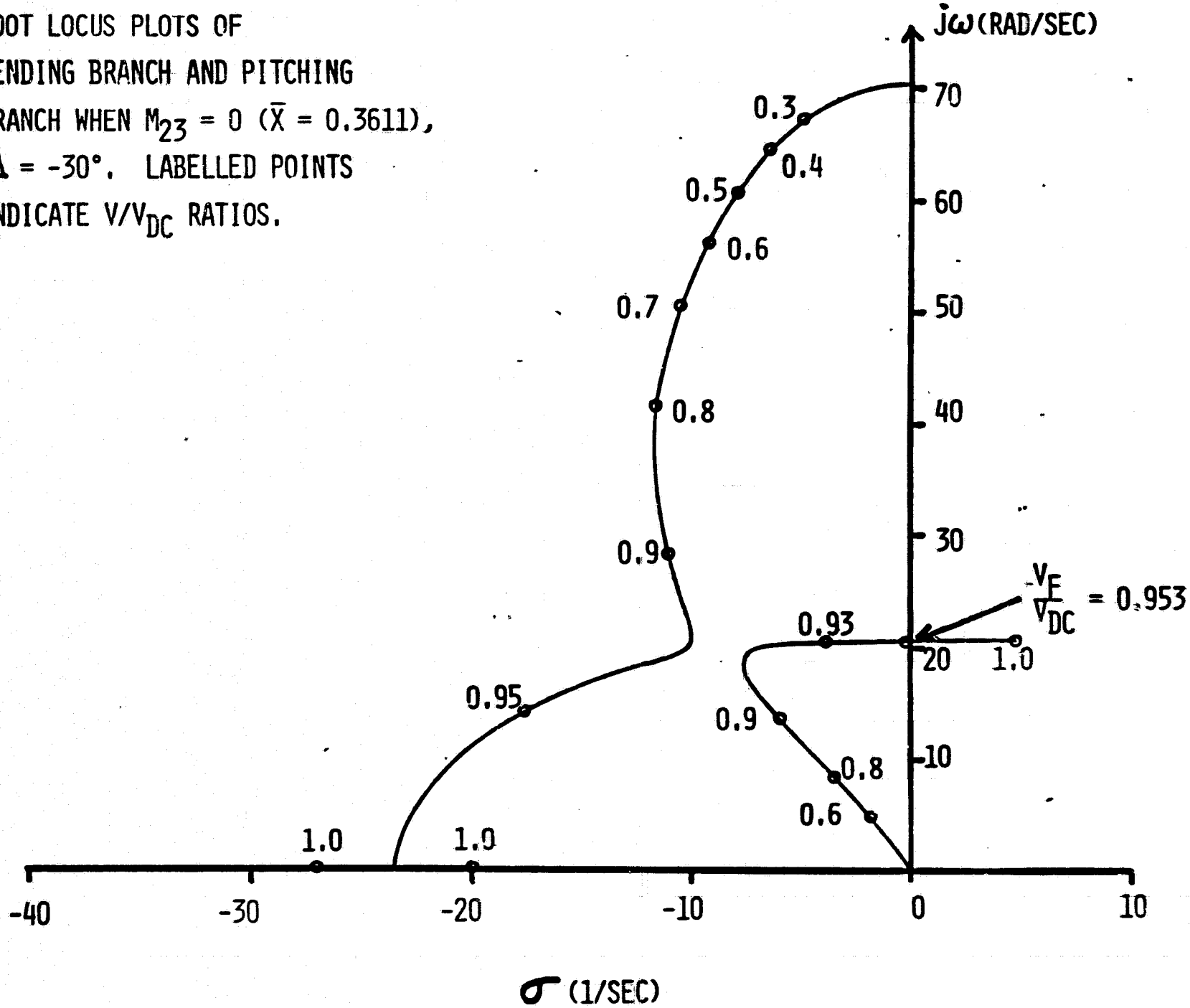

we see the transition of these characteristic root locus plots as the mass coupling changes.

Figure 6 illustrates the behavior of the bending root for $\bar{x} = 0.30$ as velocity changes. In this case, the pitch mode is statically unstable and the roots for that mode lie in the right half plane at all values of velocity. Note that the flutter frequency is relatively unchanged from other examples, but it has declined as $\bar{x}$ decreases. On the other hand, the flutter speed has increased to a little over 2% above V_{DC}.

A summary of the figures presented previously is contained in Figure 7. In this figure the ratio V_{DF}/V_{DC} is shown as the upper curve and is plotted on the left scale, against $\bar{x}$ while the ratio ω_F/ω_0 is plotted on the right, also against $\bar{x}$, and is the lower curve. Two vertical lines are drawn to indicate: the position where mass coupling between bending and pitch changes sign; and, the position, $\bar{x} = \bar{x}_s$, below which the aircraft becomes statically unstable at any speed as a rigid aircraft. Mention should be made that static aeroelastic deformation causes the aircraft to be unstable at a low q before this value $\bar{x}_s$ is reached.

An alternative to changing the wing root position is to change the wing sweep at a constant root position. We would expect to see similar behavior of the flutter speed since the longitudinal C.P. position is changing. However, in addition, we are changing the aerodynamic coupling by changing the sweep.

Figure 8 shows the results of a quasi-steady flutter study for our model where $\bar{x} = 0.40$ and Λ is varied from 0 to -50 degrees.

Figure 6

BENDING MODE ROOT LOCUS WITH $\bar{X}$ = 0.30. NOTE THAT AIRCRAFT IS STATICALLY UNSTABLE IN PITCH. CIRCLES INDICATE VALUES OF V/V_{DC}.

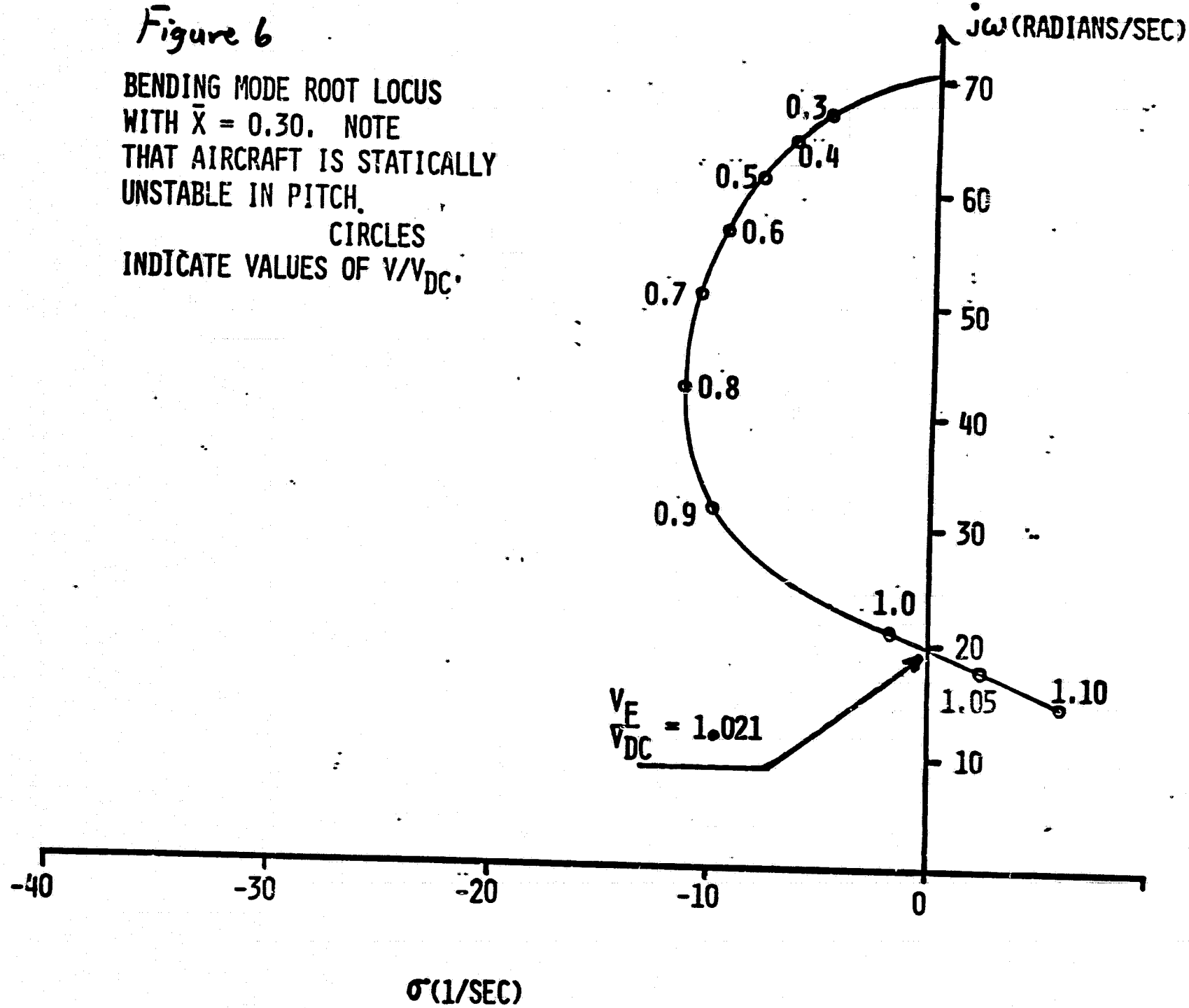

Figure 7

THE EFFECT ON FLUTTER SPEED AND FREQUENCY OF WING ROOT POSITION RELATIVE TO THE A/C C.G.

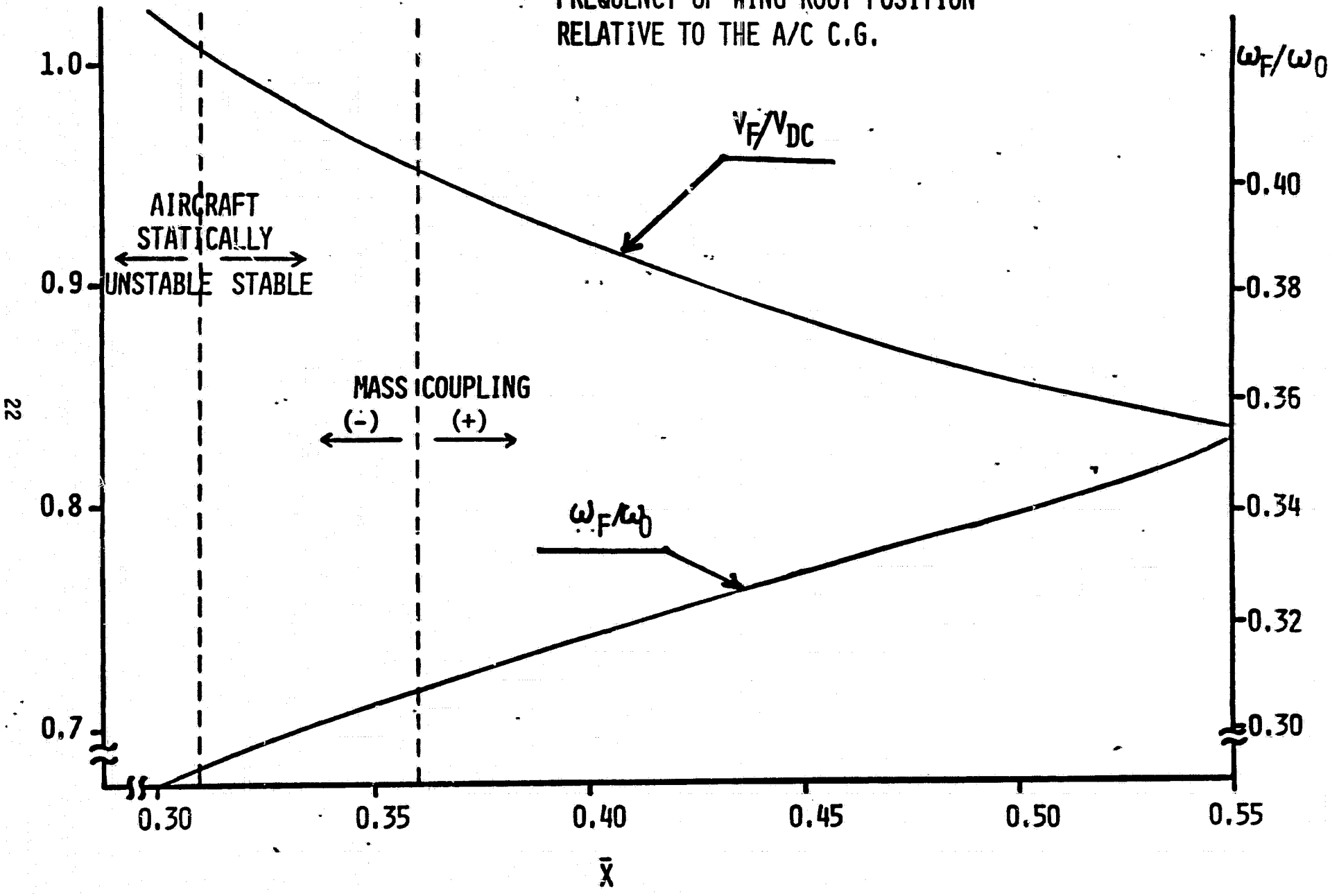

Figure 8

THE EFFECT OF WING SWEEP FORWARD WITH
$\bar{X}$ = 0.40, ALL OTHER PARAMETERS FIXED

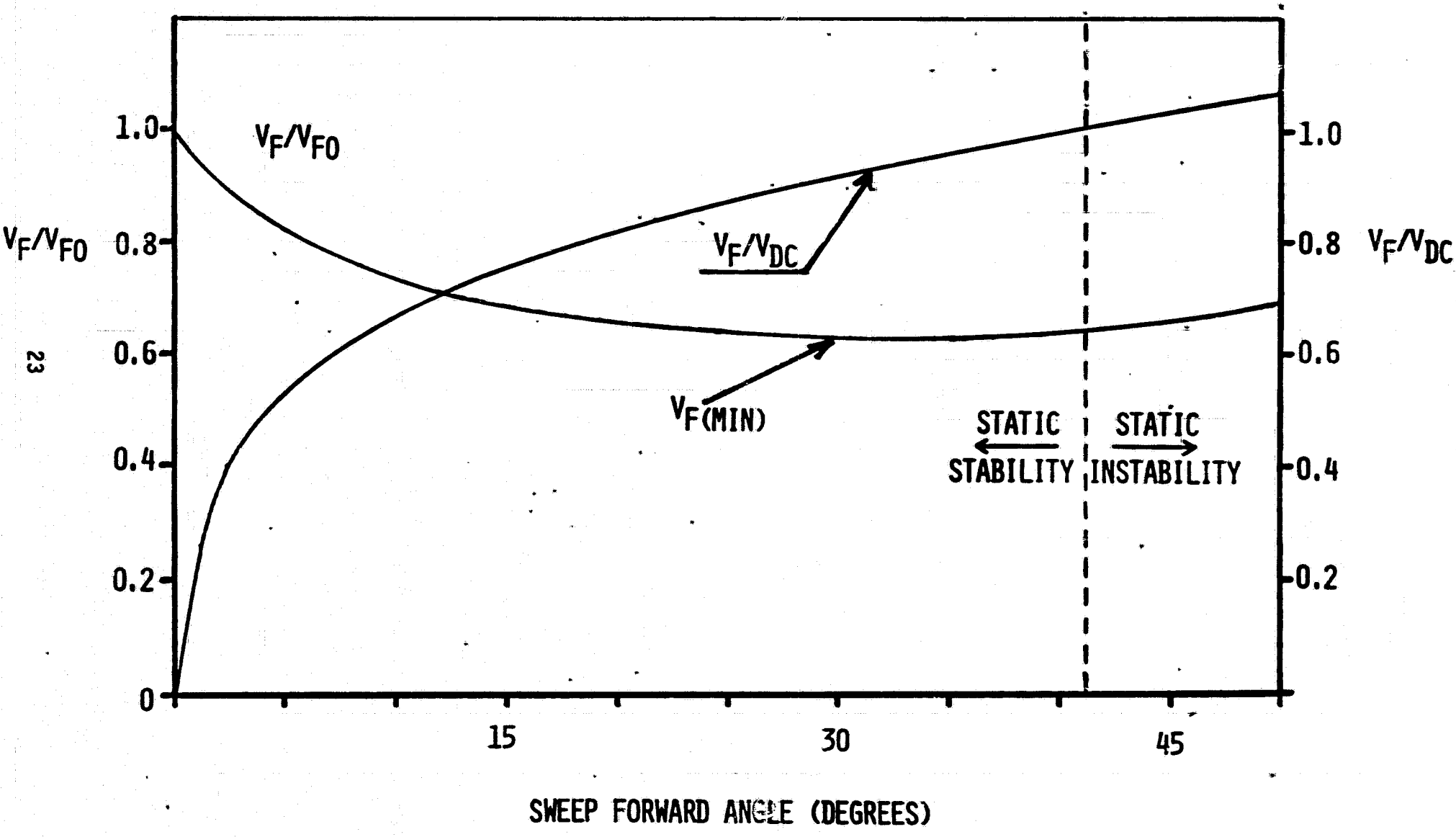

In this figure, the ratio of the body-freedom flutter speed at a given sweep angle to the body-freedom flutter speed at zero sweep is plotted. This curve, V_F/V_{FO}, begins at 1.0 when $\Lambda = 0$ and declines as the wing is swept forward. The minimum value of body freedom flutter speed is reached at $\Lambda = -30$ degrees. Thereafter, the speed increases slowly.

As the wing is swept forward, the theoretical clamped wing bending divergence speed drops rapidly (it is infinite at $\Lambda = 0$ degrees) and reaches a minimum at $\Lambda = -45$ degrees. Also shown in Figure 8 is the ratio of V_F to V_{DC}. This ratio begins at 0 when $\Lambda = 0$ and increases with forward sweep angle. A vertical line marks the transition from rigid aircraft static stability to static instability.

SUMMARY

We have seen that a forward swept wing aircraft can suffer from body freedom flutter due to coupling between bending and rigid body motions, in this case pitch and plunge. One significant parameter that determines the degree of severity of this type of flutter is the nondimensional distance $\bar{x}$. For far aft wing positions, mass coupling is introduced that tends to introduce wing inertia forces that cause nose up pitching motion as the wing vibrates upward. As the wing root is positioned closer to the aircraft c.g. this inertial coupling decreases and finally changes sign at a position $\bar{x}_o$. If the wing longitudinal CP is close to the c.g. we will have an aeroelastic instability occurring near the clamped wing divergence speed of the aircraft. However,

this instability is oscillatory, not aperiodic. While the reduced frequency of the body freedom flutter mode is small, in the range of 0.01 to 0.03, the flutter frequency is of the order of one-quarter to one-third of the fundamental bending frequency of the fixed root wing.

How closely these results from a greatly simplified model match the actual behavior of a high speed aircraft with all its complexity remains to be seen. However, a simple wind tunnel test by Foist and Sanger at Purdue in April of 1981 showed that body freedom flutter of the type described could occur. In addition, although finite span aerodynamic effects and the effects of compressibility will surely change the values of the body freedom flutter speeds calculated, the ratio of flutter speeds computed to the fixed root divergence speed should be less affected.

Finally, the significance of the fixed root wing divergence speed to the aircraft dynamic response characteristics should be discussed.

Although the mode of instability is not fixed root wing divergence, the speed V_{DC} is highly meaningful and not to be ignored. This speed is a benchmark to which all wing flexibility effects must be referred. At about 0.6 V_{DC}, the wing begins to rapidly lose its stiffness (aerodynamic plus structural). Beyond this point coupling between flexible modes and rigid body modes is likely to be significant. This coupling and decreased stiffness may have important consequences to handling qualities and fatigue life.

APPENDIX

The mass matrix [M] is:

$$[M] = \begin{bmatrix} 1 & M_{12} & M_{13} \\ \frac{2}{5}\left(\frac{\nu}{1+\nu}\right) & \frac{104}{405}\left(\frac{\nu}{1+\nu}\right) & M_{23} \\ -\frac{\nu}{1+\nu}\bar{y} & \left(\frac{-\nu}{1+\nu}\right)\left(\frac{2}{5}\bar{y}+\frac{4}{45}\sin\lambda\right) & \bar{r}^2 \end{bmatrix}$$

(Symmetric)

The aerodynamic damping matrix is [B];

$$[B] = D \begin{bmatrix} 1 & 2/5 & -\bar{y} \\ 2/5 & \frac{104}{405} & -\left(\frac{2}{5}\bar{y}+\frac{4}{45}\sin\lambda\right) \\ -\bar{y} & -\left(\frac{2}{5}\bar{y}+\frac{4}{45}\sin\lambda\right) & \bar{y}^2+\frac{\sin^2\lambda}{12} \end{bmatrix}$$

where $D = \rho\frac{v_n S C_{L\alpha}}{M_T} = 2\frac{q_n S C_{L\alpha}}{M_T l}\left(\frac{l}{v_n}\right)$

The system stiffness is composed of the sum of the aerodynamic stiffness plus the structural stiffness. [K] is computed to be:

$$[K] = Q\begin{bmatrix} 0 & \tan\Lambda & -\frac{1}{\cos\Lambda} \\ 0 & \frac{\tan\Lambda}{2} & -\frac{2}{S}\left(\frac{1}{\cos\Lambda}\right) \\ 0 & -\left(\bar{y}+\frac{\sin\Lambda}{10}\right)\tan\Lambda & \bar{y}/\cos\Lambda \end{bmatrix}$$

$$+\left(\frac{104}{405}\right)\omega_o^2\left(\frac{\nu}{1+\nu}\right)\begin{bmatrix} 0 & 0 & 0 \\ 0 & 1 & 0 \\ 0 & 0 & 0 \end{bmatrix}$$

where $Q = 2qnSC_{L\alpha}/M_T l$

A Model for an Active Canard

A model of an all-movable canard was also developed. The geometry of this canard is shown in Figure A. The effect of this canard is assumed to be aerodynamic only. Any dynamic or inertial effects are ignored. The canard induced aerodynamic forces and moments appear explicitly only in the c.g. and pitch equations of motion. The quasi-steady angle of attack of the canard surface is:

$$\alpha_c = \Theta + \delta_o - \left(\frac{\dot{w}}{V} - \frac{d\dot{\theta}}{V}\right) \qquad (3)$$

The canard lift per side is:

$$L_c = q S_c C_{L\alpha_c} \alpha_c \qquad (4)$$

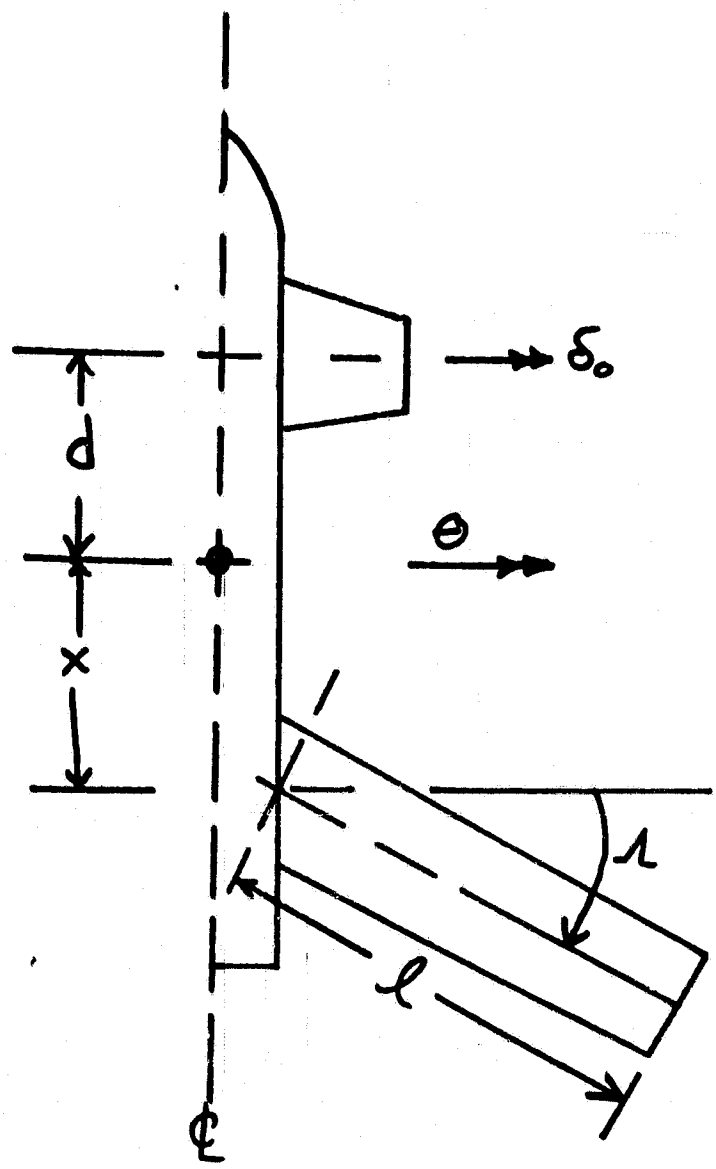

Figure A - Planform Geometry

This may be written as:

$$L_c = q S C_{L_\alpha} f (\theta + \delta_o) - \frac{1}{2} \rho v S C_{L_\alpha} f \ell (\bar{w} + \bar{d}\theta) s \tag{5}$$

where $f = S_c C_{L_{\alpha_c}} / S C_{L_\alpha}$

and $\bar{d} = d/\ell$ with $\bar{w} = w/\ell$

The pitching moment, positive nose up, is found, for each canard surface, to be:

$$M_c = \bar{d} \ell L_c \tag{6}$$

The lift and pitching moment expressions are next nondimensionalized to conform to our nondimensional equations of motion. Now, L_c contributes to the lift equation as follows:

$$\bar{L}_c = \frac{2L_c}{M_T \ell} = \begin{bmatrix} 0 & 0 & -K_{13} \end{bmatrix} \{\xi\} + \begin{bmatrix} -B_{11} & 0 & -B_{13} \end{bmatrix} \{\xi\} + \frac{2 q_\infty S C_{L_\alpha}}{M_T \ell} \left(\frac{f}{\cos^2 \Lambda} \right) \delta_o \tag{7}$$

where

$$K_{13} = -\frac{f}{\cos^2\Lambda}\left(\frac{2q_\infty S C_{L_\alpha}}{M_T l}\right) \tag{8}$$

$$B_{11} = \left(\frac{f}{\cos\Lambda}\right)\left(\frac{\rho V_\infty S C_{L_\alpha}}{M_T}\right) \tag{9}$$

$$B_{13} = \frac{\bar{d}f}{\cos\Lambda}\left(\rho V_\infty \frac{S C_{L_\alpha}}{M_T}\right) \tag{10}$$

The nondimensional pitching moment contribution to the equations of motion is:

$$\begin{aligned}\bar{M}_c = \frac{2M_c}{M_T l^2} &= \begin{bmatrix} 0 & 0 & -K_{33} \end{bmatrix}\{\zeta\} \\ &+ \begin{bmatrix} -B_{31} & 0 & -B_{33} \end{bmatrix}\{\dot{\zeta}\} \\ &+ Q\left(\frac{\bar{d}f}{\cos^2\Lambda}\right)\delta_0\end{aligned} \tag{11}$$

where

$$K_{33} = -\frac{\bar{d}f}{\cos^2\Lambda}\left(\frac{2q_\infty S C_{L_\alpha}}{M_T l}\right) \tag{12}$$

$$B_{31} = \rho V_\infty \frac{S C_{L_\alpha}}{M_T}\left(\bar{d}f/\cos\Lambda\right) \tag{13}$$

$$B_{33} = \frac{\rho V_n S C_{L_d}}{M_T}\left(\frac{\bar{d}^2 f}{\cos\lambda}\right) \tag{14}$$

The presence of the canard surface will add a set of matrix terms to the left hand side of the equations of motion.

$$[A_c] = \begin{bmatrix} 0 & 0 & K_{13} \\ 0 & 0 & 0 \\ 0 & 0 & K_{33} \end{bmatrix} \begin{Bmatrix} \xi_i \end{Bmatrix} + s \begin{bmatrix} B_{11} & 0 & B_{13} \\ 0 & 0 & 0 \\ B_{31} & 0 & B_{33} \end{bmatrix} \begin{Bmatrix} \xi_i \end{Bmatrix} \tag{15}$$

In addition, a term due to δ_0 appears on the right hand side.

$$\{F_\delta\} = Q \frac{f}{\cos^2\lambda} \begin{Bmatrix} 1 \\ 0 \\ \bar{d} \end{Bmatrix} \delta_0 \tag{16}$$

The canard deflection δ_0 is related here to the three degrees of freedom in the problem by the following relationship:

$$\delta_0 = \begin{bmatrix} C_1(s) & C_2(s) & C_3(s) \end{bmatrix} \begin{Bmatrix} \xi_i \end{Bmatrix} \tag{17}$$

where the terms C_1, C_2 and C_3 are complex functions in general. For simplicity, let

$$C_1(s) = C_{10} + s C_{11} + s^2 C_{12} \tag{18}$$

$$C_2(s) = C_{20} + s C_{21} + s^2 C_{22} \tag{19}$$

$$C_3 = C_{30} + s C_{31} + s^2 C_{32} \tag{20}$$

so that

$$\delta_0 = [C_{i0}]\{\xi_i\} + s[C_{i1}]\{\xi_i\} + s^2[C_{i2}]\{\xi_i\} \tag{21}$$

With these definitions, the canard deflection causes a set of generalized forces given by:

$$\{F_\delta\} = \frac{2 q_\infty S C_{L_\alpha}}{M_T \ell}\left(\frac{f}{\cos^2\Lambda}\right)\begin{bmatrix} C_1 & C_2 & C_3 \\ 0 & 0 & 0 \\ \bar{d}C_1 & \bar{d}C_2 & \bar{d}C_3 \end{bmatrix}\{\xi_i\} \tag{22}$$

$$\{F_\delta\} = \frac{Q f}{\cos^2\Lambda}\left[\begin{bmatrix} C_{10} & C_{20} & C_{30} \\ 0 & 0 & 0 \\ \bar{d}C_{10} & \bar{d}C_{20} & \bar{d}C_{30} \end{bmatrix} + s\begin{bmatrix} C_{11} & C_{21} & C_{31} \\ 0 & 0 & 0 \\ \bar{d}C_{11} & \bar{d}C_{21} & \bar{d}C_{31} \end{bmatrix} + s^2\begin{bmatrix} C_{12} & C_{22} & C_{32} \\ 0 & 0 & 0 \\ \bar{d}C_{12} & \bar{d}C_{22} & \bar{d}C_{32} \end{bmatrix}\right]\{\xi\} \tag{23}$$

The matrix equation of motion now becomes:

$$\left[s^2[\bar{M}] + s[\bar{B}] + [\bar{k}] \right] \{\delta\} = \{0\}$$

where $\bar{M}$, $\bar{B}$ and $\bar{K}$ represent the augmented system matrices, given by:

$$[\bar{M}] = [M] - \frac{\bar{Q} f}{\cos^2 \Lambda} [\bar{C}]^{(2)} \tag{26}$$

$$[\bar{B}] = [B^*] - \frac{\bar{Q} f}{\cos^2 \Lambda} [\bar{C}]^{(1)} \tag{27}$$

$$[\bar{K}] = [K^*] - \frac{\bar{Q} f}{\cos^2 \Lambda} [\bar{C}]^{(0)} \tag{28}$$

$[B^*]$ and $[K^*]$ include the canard damping and stiffness, respectively, with the control locked ($\delta_0 = 0$).

The augmented mass, damping and stiffness matrices are:

$$[\bar{M}] = \left[\begin{array}{c|c|c} 1 - \bar{Q} C_{12} & \frac{2}{5}\left(\frac{\nu}{1+\nu}\right) - \bar{Q} C_{22} & \frac{-\nu \bar{y}}{1+\nu} - \bar{Q} C_{32} \\ \hline \frac{2}{5}\left(\frac{\nu}{1+\nu}\right) & \frac{104}{405}\left(\frac{\nu}{1+\nu}\right) & \frac{-\nu}{1+\nu}\left(\frac{2}{5}\bar{y} + \frac{4}{45}\sin\Lambda\right) \\ \hline \left(\frac{-\nu}{1+\nu}\right)\bar{y} - \bar{Q}\bar{d}C_{12} & \left(\frac{-\nu}{1+\nu}\right)\left(\frac{2}{5}\bar{y} + \frac{4}{45}\sin\Lambda\right) - \bar{Q}\bar{d}C_{22} & \bar{F}^2 - \bar{Q}\bar{d}C_{32} \end{array}\right]$$

where $\bar{Q} = 2q_n\, SC_{L\alpha} f/(M_{T\ell} \cos^2\Lambda) = 2q\, SC_{L\alpha} f/M_{T\ell}$

$$[\bar{B}] = \begin{bmatrix} D\left[1 + f/\cos\Lambda\right] - \bar{Q}C_{11} & \frac{2}{5}D - \bar{Q}C_{21} & D\bar{d}f/\cos\Lambda - \bar{Q}C_{31} - \bar{y}D \\ \frac{2}{5}D & \frac{104}{405}D & -D\left(\frac{2}{5}\bar{y} + \frac{4}{45}\sin\Lambda\right) \\ D\bar{d}f/\cos\Lambda - \bar{Q}\bar{d}C_{11} - \bar{y}D & -D\left(\frac{2}{5}\bar{y} + \frac{4}{45}\sin\Lambda\right) - \bar{Q}\bar{d}C_{21} & D\left(\bar{y}^2 + \frac{\sin^2\Lambda}{12}\right) - \bar{Q}\bar{d}C_{31} + \bar{d}^2 f D/\cos\Lambda \end{bmatrix}$$

where $D = \rho V_n\, SC_{L\alpha}/M_T$

Finally, the augmented stiffness matrix is:

$$[\bar{K}] = \begin{bmatrix} -\bar{Q}C_{10} & Q\left(\tan\Lambda - \frac{f}{\cos^2\Lambda}C_{20}\right) & -\bar{Q}fC_{30} - \bar{Q}f - Q/\cos\Lambda \\ 0 & Q\frac{\tan\Lambda}{2} + \frac{104}{405}\omega_0^2\left(\mu/(1+\mu)\right) & -\frac{2}{5}Q/\cos\Lambda \\ -\bar{Q}\bar{d}C_{10} & -Q\left(\bar{y} + \frac{\sin\Lambda}{10}\right)\tan\Lambda - \bar{Q}\bar{d}fC_{20} & Q\left[\frac{\bar{y}}{\cos\Lambda} - \frac{\bar{d}f}{\cos^2\Lambda} - \frac{\bar{d}f}{\cos^2\Lambda}C_{30}\right] \end{bmatrix}$$

References

1. R.A. Fraser and W.J. Duncan, "Wing Flutter as Influenced by the Mobility of the Fuselage," British Aero. Research Council, R. & M. No. 1207, 1929.

2. E.G. Broadbent, "Some Considerations of the Flutter Problems of High Speed Aircraft," Second International Aircraft Conference, N.Y. 1949, pp. 556-581.

3. D.R. Gaukroger, "Wind Tunnel Flutter Tests on Model Delta Wing under Fixed and Free-Root Conditions," British A.R.C. R & M. 2826, 1955.

4. D.R. Gaukroger, "Wind Tunnel Tests on the Symmetric and Anti-symmetric Flutter of Sweptback Wings," British A.R.C, R. & M. 2911, 1955.

5. D.R. Gaukroger, "Wing Flutter," AGARD Manual on Aeroelasticity Part V, Chapter 2, 1960.

6. H.J. Cunningham and R.R. Lundstrom, "Description and Analysis of a Rocket-Vehicle Experiment on Flutter Involving Wing Deformation and Body Motions," NACA TN 3311, January 1955, (originally done published as NACA RM L50 I29, 1950).

7. G.J. Hancock, "The Static Aeroelastic Deformation of Slender Configurations, Part III: Static Stability, "The Aeronautical Quarterly, Vol. XIV, February 1963, pp. 75-104.

8. G.J. Hancock, "Static Aeroelasticity - A Reappraisal", Proceedings of the AIAA Symposium on Structural Dynamics and Aeroelasticity, Boston, Mass., 1965.

9. S.I. Pai and W.R. Sears, "Some Aeroelastic Properties of Swept Wings," Journal of the Aeronautical Sciences, Feb. 1949, pp. 105-115, 119.